JOURNAL OF CATALYSIS **162,** 66–75 (1996)
ARTICLE NO. 0260

Catalyst Preparation Variables That Affect the Creation of Active Sites for HDS on $Co/Mo/Al_2O_3$ Catalytic Materials

Michiaki Adachi,* Cristian Contescu,† and James A. Schwarz‡

Department of Chemical Engineering and Materials Science, Syracuse University, Syracuse, New York 13244-1190

Received October 26, 1995; revised April 18, 1996; accepted April 19, 1996

In a recent paper (*J. Catal.* 158, 411, 1996) we demonstrated that the intensity of a specific peak (pK $\sim$6) in proton affinity distributions (PADs) measured for a series of $Co\text{-}Mo/Al_2O_3$ catalysts could be correlated to the variation in HDS activity within the series. PADs access information about species on the catalyst's surface from analyses of proton binding data collected using potentiometric titration. If the species determined at the solid/aqueous interface are present after catalyst activation and are active during catalytic testing, then this methodology can provide a simple, surface sensitive procedure for catalyst characterization which should correlate with other characterization techniques. To test this hypothesis we provide herein results from more conventional catalyst characterization techniques in order to corroborate the PAD results. The techniques of temperature-programmed reduction, X-ray photoelectron spectroscopy, and laser Raman spectroscopy were used to provide additional characterization of $Co\text{-}Mo/Al_2O_3$ catalysts in their oxide state. PADs were obtained for this catalyst system in their oxide and sulfided states. The HDS activity for each member of this series was measured using hydrodesulfurization of thiophene as a test reaction. The effect of cobalt loading, molybdenum content, presulfidation conditions, and pH during catalyst preparation were the variables used. Based on the experimental data we propose that the active site for HDS activity is a Co-Mo interaction species consisting of molybdate octahedra and a dispersed Co which could also be octahedrally coordinated. This species can be transformed reversibly during the processes of sulfidation and reoxidation and its formation is controlled by pH.

INTRODUCTION

Hydrotreating catalysts have played an important role in producing clean fuels without heteroatoms and aromatic compounds. Although Mo catalysts promoted by Co and/or Ni are used worldwide, the nature of the active sites on the catalysts has been under discussion for a long time (1–3).

Structures on the sulfided catalysts have been characterized by various techniques in order to establish a relationship between them and catalyst activity under working conditions. A "Co-Mo-S" model was proposed by Topsøe and coworkers (4, 5) on the basis of the data acquired by using Mössbauer emission spectroscopy (MES). Using extended X-ray absorption fine structure (EXAFS), Niemann *et al.* (6) proposed the square-pyramidal model for Co-Mo-S (Ni-Mo-S). Later, Louwers and Prins (7) provided additional EXAFS evidence for this model. The study of hydrodesulfurization of dibenzothiophene using radioisotope ^{35}S tracer was conducted by Kabe and coworkers and their results supported the existence of the "Ni-Mo-S" structure (8). On the other hand, using MES, Crajé and coworkers have proposed that Mo is not needed to form a Co-Mo-S phase because dispersed Co on Mo shows a high HDS activity, which resulted in their proposal that Co sulfide can be highly dispersed on the Mo sulfide (9).

Characterization of the promoted hydrotreating catalyst in the oxide state has not been conducted as extensively as in the sulfided state. It is well known that cobalt can exist in various forms in the oxide state on the HDS catalyst. These include $CoAl_2O_4$, Co_3O_4, and octahedral Co which interacts with Mo oxide (10). These species are transformed after presulfiding. For example, Co_3O_4 was transformed into Co_9S_8 and the octahedral Co was transformed into Co in the "Co-Mo-S" phase. The tetrahedral Co in $CoAl_2O_4$ did not change after presulfiding (10). It was also found that the reactivity was determined by the structures present before sulfiding. Concerning the interaction between Co and Mo in the oxide state, some models have been proposed such as "Mo_4Co" (11) and "double layers" (12). Although the characterization of the Co (or Ni)-Mo catalysts in the oxide form using spectroscopic techniques such as IR spectra of adsorbed NO (13), ion scattering spectroscopy (ISS) (14, 15), EXAFS (16, 17), laser Raman spectroscopy (LRS) (18, 19), and X-ray photoelectron spectroscopy (XPS) (19) have been conducted, they provide only limited information about the surface structure of the oxide.

We have conducted studies (20, 21) of single transitional metal oxides (TMOs) supported on γ-Al_2O_3 with the objective of elucidating the structure of the TMO based on its proton binding chemistry on the surface; structure/activity

* Permanent address: Central Technical Research Laboratory, Nippon Oil Co., Ltd., 8 Chidori-cho, Naka-ku, Yokohama, 231 Japan.

† Permanent address: Institute of Physical Chemistry of Romanian Academy, Spl. Independentei 202, Bucharest 77208, Romania.

‡ To whom correspondence should be addressed.

0021-9517/96 $18.00

relationships were not investigated. The oxidic form present after calcination undergoes complex protolytic equilibria which are pH dependent. Using the experimental and computational methods developed for determining proton affinity distributions (PADs), we recently extended our studies to various oxide precursors of a series of Co-Mo/Al_2O_3 HDS catalysts (22). We found that new features occurred in the PADs and that their abundance was a function of the order of impregnation of the support, the promoter, and the weight loading. In all cases the appearance of a peak at pK ~ 6 could be correlated with the HDS activity, using thiophene as a reactant, of the sulfided catalyst.

Many variables exist in the causal chain designated as catalyst preparation. The effect of some of those were studied in our earlier publication (21, 22) and were correlated with PAD data and HDS activity. The results demonstrated the utility of this "absolute" surface sensitive technique to provide reliable data for correlating activity with preparation prior to sulfidation of the catalyst. However, pH has always been considered the master variable and its effects were not studied. One objective of this paper is to extend the range of variables to pH, which might be important in forming a specific structure of the precursor on a γ-alumina carrier that may be active in HDS catalysis and assess the physical and catalytic properties of the materials formed. Another objective is to demonstrate that PAD data are consistent with data retrieved from more conventional techniques thus enabling rapid and inexpensive characterization of catalysts prepared under different protocols.

EXPERIMENTAL

Catalyst Preparation

The supported catalysts used in this study were prepared by incipient wetness of an Al_2O_3 extrudate (1/16 in. D) with a BET surface area of 220 m^2/g and pore volume of 0.66 cm^3/g by using aqueous solutions of ammonium hyptamolybdate ($(NH_4)_6Mo_7O_{24} \cdot 4H_2O$ (AHM), Aldrich Chemicals) and cobalt salts. The Co salts were either $Co(NO_3)_2 \cdot 6H_2O$ (Fluka) or $Co(CH_3COO)_2 \cdot 4H_2O$ (Mellinckrodt). When the pH of the Co solution was changed (pH = 2.0, 5.3, 7.3), the latter salt was used to prevent deposition/precipitation of Co hydroxide at high pH. The motivation for using the master variable (pH) was based on results which demonstrated that TMOs supported on a carrier such as γ-alumina can undergo structural changes under ambient conditions which correlate with the corresponding structures formed by hydrolysis of the transition metal salt used during catalyst preparation. (20, 23). Thus, by systematic variation of the pH during catalyst preparation, it is potentially possible to produce new structure(s) on the catalyst subsequent to calcination. Successive impregnation (first Mo, second Co, C-M) were used to prepare Co-Mo/Al_2O_3 catalysts. Catalysts, which contained one of the two components, were also prepared. The samples' designation and metal content are given in Table 1. Except where noted in the text, all references to Co-Mo/Al_2O_3 catalysts will be for the nominal Mo loading of $\sim$15 wt% in which the Co precursor was the nitrate. All weight loadings are reported on an oxide basis. After impregnation, the samples were kept at room temperature overnight before drying at 393 K for 12 h. Calcination was conducted in a muffle furnace by ramping at the rate of 10 K/min to 823 K and holding for 4 h, following another hold at 473 K for 1 h. When successive impregnation was used the second impregnation was conducted after calcination and this catalyst was calcined, as described above, before testing.

TABLE 1

Sample List

Nomenclature	MoO_3 wt%	CoO wt%	Co salt
A	4.7	0	None
B	4.7	1.1	Nitrate
C	14.6	0	None
D	14.4	1.2	Nitrate
E	14.1	3.3	Nitrate
F	14.0	4.6	Nitrate
G	13.6	6.7	Nitrate
H	15.5	3.8 (pH 2.0)	Acetate
I	15.5	3.8 (pH 5.3)	Acetate
J	15.5	3.8 (pH 7.3)	Acetate

Note. The numbers in parentheses are the pH of the cobalt solution used for the impregnation.

Titration Procedure

The experimental procedure used for potentiometric titration is described in detail elsewhere (20–22). A 665 Dosimat (Metrohm) microburette, a thermostated titration vessel and a digital Fisher Accumet Model 50 pH meter equipped with a combination glass electrode were used for the measurement. All experiments were conducted under a nitrogen atmosphere at constant temperature (298 K), and constant ionic strength (0.01 *N* $NaNO_3$). The solid samples (0.5 g) were titrated after equilibration with the inert electrolyte solution (initial volume, V_0). The procedure consisted of adding acid increments (V_a) of titrant and/or base increments (V_b) to the well-agitated suspension and collecting the equilibrium pH data at regular time intervals. The titrant used was either NaOH or HNO_3 solution (volume, V_t) whose normality was 0.1. The proton consumption function was calculated as

$$H_{cons} = V_0(C_a - C_b) + 0.1(V_a - V_b) - (V_0 + V_t)\{[H]_f - [OH]_f\}$$

from the analytical concentrations of acid (C_a) and/or base (C_b) and from the actually measured concentrations of H^+ or OH^-. The proton consumption function was then normalized with respect to the amount of the titrated sample.

When titration of the sulfided samples was conducted, they were placed in the vessel which contained the 0.01 *N* $NaNO_3$ solution, and blanketed with a nitrogen atmosphere in advance to prevent contact with air.

Method of Calculation of the Proton Affinity Distribution (PAD)

The method for calculation of the affinity distribution function was described in previous publications (20, 21, 24). The same numerical procedures were used for all samples titrated, including the Al_2O_3 support. A subtle, but important, distinction requires a brief comment, a more expanded discussion can be found in our analysis of the WO_3/Al_2O_3 system (20). For Al_2O_3, the proton binding/release occurs on surface hydroxyl groups in specific ranges of pH that can be related to the crystallo-chemical coordination of OH to aluminum ions in the lattice (21, 24); the local isotherm is considered to be of Langmuir form. On the other hand, in acid–base titration of polyprotic systems, the first derivative of the overall binding curve shows the tendency of the system, at equilibrium, to resist a pH change for an incremental addition of constituent; this effect is known as the buffering intensity. The buffering power may be similarly defined for hydrolizable systems (25). Each hydrolysis species contributes to the buffer intensity and usually no steps occur in the binding curve because successive acidity constants are close to each other.

In general terms, a distribution function of proton lability for a non-uniform oxide surface, $f(\mathrm{pK})$, can be defined as the mole fraction of surface sites with acidity constants in the interval $(\mathrm{pK}, \mathrm{pK} + d\,\mathrm{pK})$. For a system composed of several groups of proton binding sites, the total concentration of deprotonated sites is given by

$$\Theta = \int_{\mathrm{pK}_1}^{\mathrm{pK}_2} \left[\theta\left([\mathrm{H}], \mathrm{pK}\right)\right] f(\mathrm{pK})\, d\,\mathrm{pK}, \qquad (1)$$

where the bracketed term in the integral takes the form of a Langmuir local isotherm with the corresponding proton binding constant, K^{-1}. It corresponds to proton transfer processes between amphoteric surface hydroxyls, such as those on γ-Al_2O_3, and the aqueous electrolyte solution; they are usually described by simple local equlibria which are structurally dependent:

$$\equiv\mathrm{M\text{-}OH}^{+1/2} \overset{K_{\mathrm{M\text{-}OH}}}{\Longleftrightarrow} \equiv\mathrm{M\text{-}O}^{-1/2} + \mathrm{H}^+ \qquad (\mathbf{I})$$

When complex protolytic equilibria are involved, such as

$$\equiv\mathrm{M}_x\mathrm{H}_y\mathrm{O}_z(\mathrm{OH})_w^{t-} + \gamma\,\mathrm{H_2O} \overset{Q_\beta}{\Longleftrightarrow} \alpha\equiv\mathrm{MO}_4^{2-} + \beta\mathrm{H}^+ \qquad (\mathbf{II})$$

which for $M = \mathrm{W}$ or Mo depicts the octahedral-to-tetrahedral transformation of aggregates generated by these network forming oxides, an apparent hydrolytic equilibrium constant can still be defined in terms of the hydrolysis quotient, Q_β, as $K_{\mathrm{hydr}} = (Q_\beta)^{1/\beta}$.

All proton-transfer processes described above are pH dependent. In accordance with the above description, it appears that potentiometric titration is a simple and versatile experimental method which is well suited for evaluation of surface structures on solid samples which undergo proton transfer to or from the aqueous environment.

Quantitative evaluation of the component peaks in the PAD function, $f(\mathrm{pK})$, was done by decomposing them with Gaussian functions. The area under the peaks, which represents the amount ($\mathrm{mmol} \cdot \mathrm{g}^{-1}$) of surface sites available for proton binding/release processes within the corresponding pH range, was evaluated using Peakfit software. The accuracy of this approach is estimated to be ±5% based on experimental data from homogeneous titration of model compounds (24).

Thiophene Hydrodesulfurization

The hydrodesulfurization of thiophene was conducted in a flow system using a microreactor operating at atmospheric pressure. Sulfidation of the catalyst was conducted in the same system. The particle size of the catalyst was 0.1–0.4 mm (40–80 mesh). Samples of 0.5 g, on the basis of oxide, were sulfided in a flow of 30 cm^3/min—10% H_2S/H_2 at several conditions (temperature and time). For catalytic tests a gas mixture of 2.46% thiophene (Aldrich Chemical) in H_2 was fed into the U-shaped quartz reactor at the rate of 40 cm^3/min. The reaction temperature was raised from 573 K to 613 K stepwise and was held at 613 K for 1 h. Thiophene was introduced using a bubbler system and the mole percentage was kept constant in the feed. The concentrations of thiophene in the reactant and the product were analyzed by an on-line gas chromatograph. The thiophene conversion was calculated using these values. The separation of thiophene from hydrocarbons and hydrogen sulfide was conducted under ramping conditions by using a packed column of 23% SP-1720 on 80/100 chromosorb PAW (Supelco).

XPS

The XPS spectra were obtained using a PHI 5600ci instrument. Monochromatized Al K_α (1486.6 eV) X rays were used at a power of 400 W, and the vacuum inside the analysis chamber was typically less than 5×10^{-9} Torr. The pass energy of the analyzer was 58.7 eV. The powdered samples were attached to Ag sample coupons using double-sided sticky tape. A low-energy electron flood gun was used for charge neutralization. Peak areas were measured using an integral background.

Raman Spectroscopy

Raman spectra of the calcined samples were recorded under ambient conditions with a RFS100 FT-Raman spectrometer (Bruker). A Nd-YAG laser (1064 nm) was used as the excitation source and the laser power was 20–30 mW. The spectra were obtained after 300–500 scans at a resolution of 4 cm^{-1}.

Temperature-Programmed Reduction

The TPR apparatus consisted of a quartz reactor and a thermal conductivity detector. The reducing gas was a mixture of H_2 and Ar (8 vol% H_2). Before each run, the samples were preheated in 35 cm^3/min flow of Ar at 423 K for 1.5 h. Then they were cooled to 303 K and reduced in 35 cm^3/min flow of the gas mixture while ramping the temperature from 323 K to 893 K at 10 K/min. The sample amount was constant at 52 μmol of Mo oxide and was kept constant for all runs.

RESULTS

Effect of Co Content

Although interpretation of XPS results to obtain information about catalyst dispersion has uncertainties due to the large escape depth of photoelectrons, Okamoto *et al.* (26) have applied this method to measure the concentration of Group VIII metals on the surface of hydrotreating catalysts with some success (26). Qualitative information about the relative dispersion of Co can be obtained by comparing the Co_{2p}/Al_{2p} XPS intensity ratio. Figure 1 plots this ratio as a function of the Co content for the samples. The Co-Mo samples show a linear behavior with Co concentrations up to ~5%. A similar result was reported by Okamoto *et al.* (26). However, the plot deviates from the linear relationship when the Co content is 6.7 wt%. Dufresne *et al.* (19) interpretted their Raman data for Ni-Mo/Al_2O_3 on the basis that aggregated $NiMoO_4$ occurred at high Ni loading

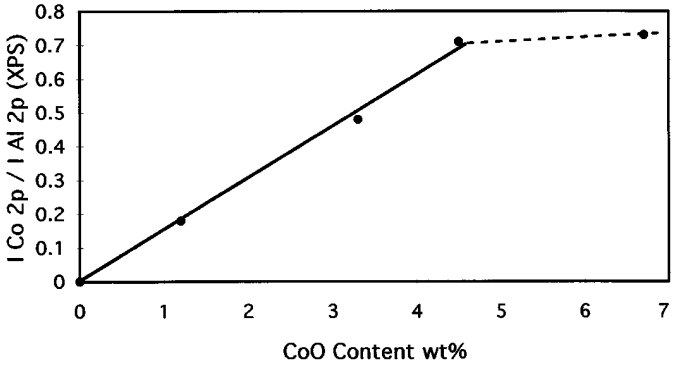

FIG. 1. Co/Al (XPS) intensity as a function of CoO content. All samples prepared by successive impregnation of Co on the same Mo/Al_2O_3.

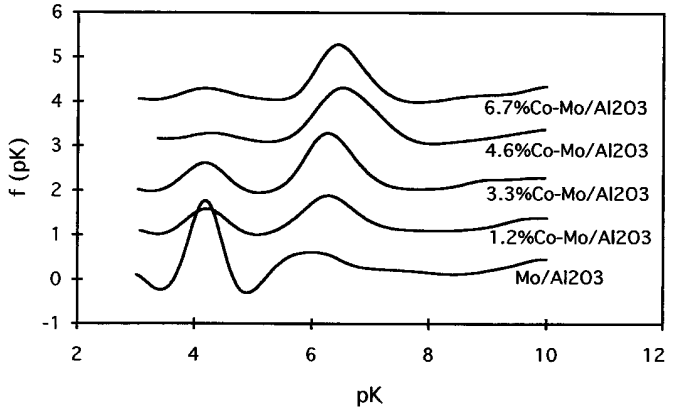

FIG. 2. Proton affinity distribution of Co-Mo/Al_2O_3 catalysts as a function of Co content. All samples prepared by successive impregnation of Co on the same Mo/Al_2O_3.

(~7%) while Ni species were well dispersed at lower Ni content samples. Using ISS, Kasztelan *et al.* (15) found similar trends for Co-Mo/Al_2O_3 as we report in Fig. 1. We conclude that added Co is dispersed when its weight loading is less than ~5 wt% and it is aggregated on the surface of the catalyst when its content exceeds this value. The Co_{2p}/Al_{2p} intensity ratio of the Co/Al_2O_3 catalyst is much less than that of the Co-Mo catalyst although the Co content is similar. The Co $2p_{3/2}$ binding energy is constant at around 781.5 eV for all the Co-Mo catalysts.

Figure 2 shows the effect of added Co on the PAD of a Mo/Al_2O_3 sample whose Mo content is ~15 wt%. The peak centered around pK 6 increases in area as the content of Co increases up to 4.6 wt%. The data presented in this figure reproduces our previous results (22). However, when the content of Co is further increased up to 6.7 wt%, quantitative analysis of peak area revealed it to be slightly smaller than that of the catalyst whose Co content is 4.6 wt%. The HDS activity of this series followed a similar trend. Figure 3 shows the effect of the Co content on the peak area **and** HDS activity. The peak area was calculated using the Peakfit® program and normalized to the weight of catalyst. The results shown in Fig. 3 cannot be viewed as quantitative; they simply demonstrate a trend that the number of sites which give rise to a feature at pK ~6 in the PADs of the catalysts studied correlate with the HDS activity. Both measurements are a function of the Co content of the catalysts.

Figure 4 presents the TPR patterns of Co-Mo catalysts with ~15 wt% Mo and varying amounts of Co organized to emphasize the effect of the Co content. The general shape and the maximum temperatures of the profiles are not strongly dependent on the Co content up to 4.6 wt%. However, there is a down-shift in the temperature of the peak maximum which is most apparent for the 4.6 wt% Co catalyst when compared to those with less Co. On the other hand, the catalyst which contains 6.7 wt% Co has a lower

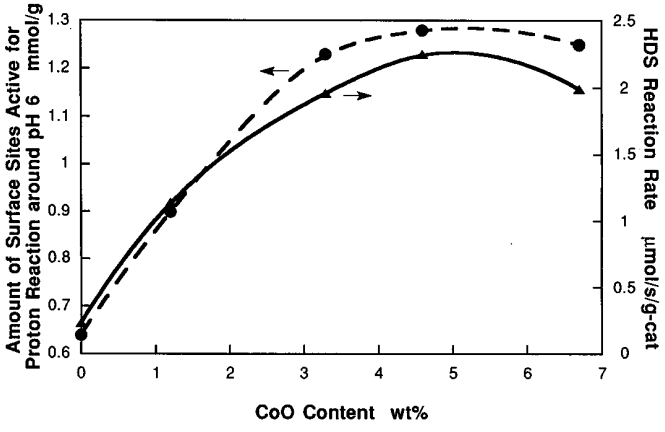

FIG. 3. Amount of surface sites active for proton reaction around pH 6 and thiophene HDS activity as a function of Co content. All samples prepared by successive impregnation (first Mo, second Co). Reaction conditions: 613 K, 1 atm, 2.46% thiophene in H_2, 0.2 g-cat.

temperature shoulder (around 653 K) when compared to catalysts with lower Co loadings. This suggests that above a certain weight loading of Co, when the support contains ~15 wt% Mo, an amount of Co cannot be accommodated intimately with Mo and thus undergoes a type of phase separation. Analyses of the areas under the TPR curves in the temperature range 623 K to 773 K showed the area increased linearly with Co loading up to 4.6 wt%. A linear relation, in what might be considered a dilute limit, is consistent with both PAD and XPS results. The linear increase may be due to the reduction of a Co–Mo interaction species (PAD results) or a hydrogen spillover effect due to an increase in Co dispersion (XPS result).

Effect of pH of the Co Solution

In order to compare results for catalysts prepared using different Co precursors, we should first demonstrate that the precursor used during preparation did not significantly

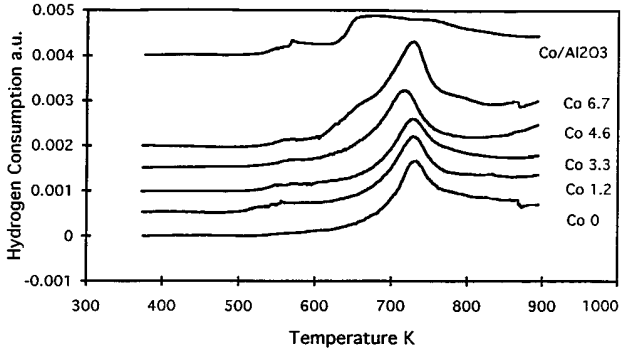

FIG. 4. Temperature-programmed reduction of Co-Mo/Al_2O_3 and Co/Al_2O_3 catalysts as a function of Co content. Co-Mo/Al_2O_3 samples prepared by successive impregnation of Co on the same Mo/Al_2O_3 which has 14.6 wt% Mo (oxide basis).

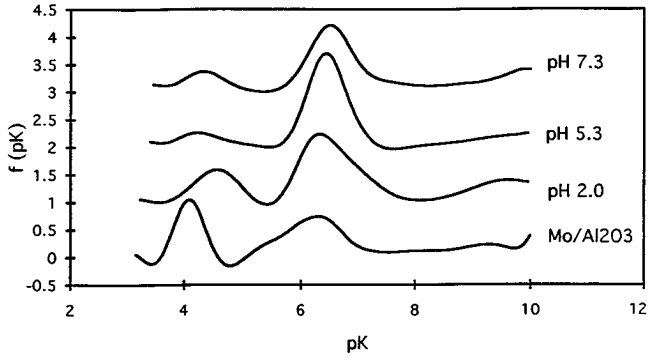

FIG. 5. Proton affinity distribution of Co-Mo/Al_2O_3 catalysts as a function of pH of Co impregnation solution. All samples prepared by successive impregnation. The content of Mo and Co is fixed at 15.5 wt% and 3.8 wt% (oxide base), respectively.

influence catalytic activity. The Co-Mo catalyst containing 4.6 wt% Co and prepared at pH ~5.2 using Co $(NO_3)_2$ as a precursor can be compared to that formed from $Co(CH_3COO)_2$ with pH ~5.3; both contain ~15 wt% Mo. For the former the thiophene conversion was ~65% while for the latter the conversion was also ~65%. This finding suggests that in our system, the activity is not strongly dependent on the Co precursor.

Figure 5 shows the PADs of the Co-Mo catalysts which were prepared from cobalt acetate solutions at different pH values. The shapes of the PADs do not differ qualitatively; however, the peak intensity around pK 6 does. The catalyst prepared using the Co solution of pH 5.3 has a larger peak area around pK 6 than the other catalysts.

In Fig. 6 we show the number of sites for proton binding around pK 6 and the HDS activity as a function of the Co solution pH. A maximum is found in both curves around pH 5 and the result demonstrates there exists some correlation between the preparation conditions, i.e., pH of impregnating solution, the surface concentration of structures that undergo a specific protolysis process (see scheme **II**), and the HDS activity of the catalyst. We postpone further comments until the Discussion.

Effect of Mo Content

Figure 7 shows the PADs of the Co-Mo catalysts which contain the same amount of Co (1 wt%) and different amounts of Mo. The low Mo content catalyst (~5 wt%) does not have a well-resolved peak around pK 6; the high Mo content catalyst (~15 wt%) shows an intense peak. Moreover, the former catalyst has a lower thiophene conversion rate (5×10^{-4} mmol $\cdot s^{-1} \cdot$ (g-cat)$^{-1}$) than the latter (1.2×10^{-3} mmol $\cdot s^{-1} \cdot$ (g-cat)$^{-1}$) (22).

Figure 8 shows the Raman spectra of two Mo/Al_2O_3 catalysts before Co impregnation. The spectra were recorded after exposure of the calcined catalyst to the ambient. Under these conditions Mo species are transformed to

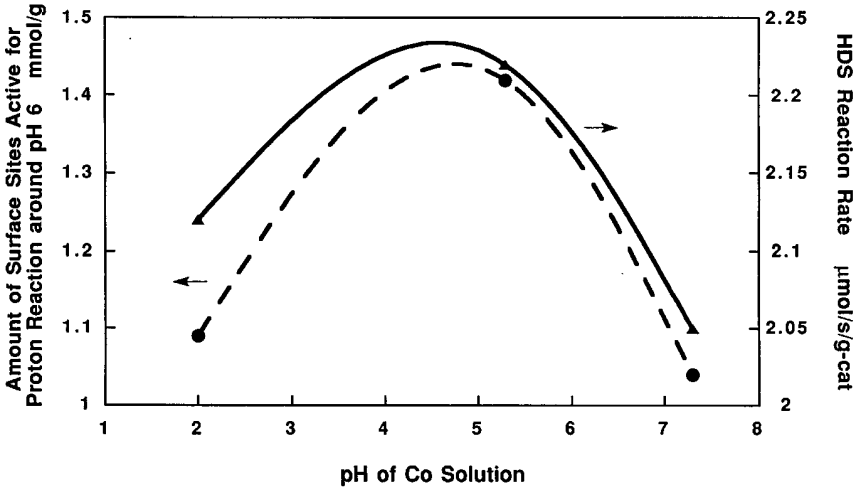

FIG. 6. Effect of pH of Co impregnation solution on thiophene HDS activity and amount of surface sites active for proton reaction around pH 6. All samples prepared by successive impregnation. The content of Mo and Co is fixed at 15.5 wt% and 3.8 wt% (oxide base), respectively.

molybdate species (18). The catalyst containing ~15 wt% Mo has an intense peak at ~950 cm^{-1}, which was reported to be a bridged or two-dimensional polymeric form of distorted molybdate octahedra (27, 28). On the other hand, the low Mo content catalyst only has a small, not well-defined, peak in this region. In this case, apparently only a small amount of octahedral molybdate exists on the surface of the catalyst and tetrahedral molybdate dominates (29).

Presulfidation

The method of potentiometric titration was previously used in the study of proton binding equilibria on metal sulfides (30, 31); it was shown that the approach used to interpret the charge-pH behavior of hydrated oxides could be extended to hydrated sulfided phases, too.

Figure 9 shows the effect of presulfiding condition on the PAD of a Co-Mo/Al_2O_3 with 3.3 wt% Co and ~15 wt% Mo. The peak around pK 6 decreases in area as the presulfiding condition becomes more severe. Clearly the proton chemistry occurring in this complex protolytic equilibria is affected by the presence of sulfur. Increasing the severity of the sulfiding conditions could result in increasing the sulfur content of the surface Co-Mo species which gives rise to the feature at pK ~ 6 found on the unsulfided starting material. We attribute the decrease to the formation of a Co-Mo-S compound whose hydrolysis would either be different from the oxidic analog or non-existent in the pH window of investigation. When sulfidation is conducted at temperatures over 623 K, the peak at ~pK 4 increases in area concomitant with the decrease of the peak ~pK 6. The peak at pK ~4 corresponds to that which was found only on γ-Al_2O_3 alone (22, 24). After reoxidation at 873 K for 4 h, following the presulfiding at 673 K for 2 h, the PAD pattern of the unsulfided catalyst is completely reproduced.

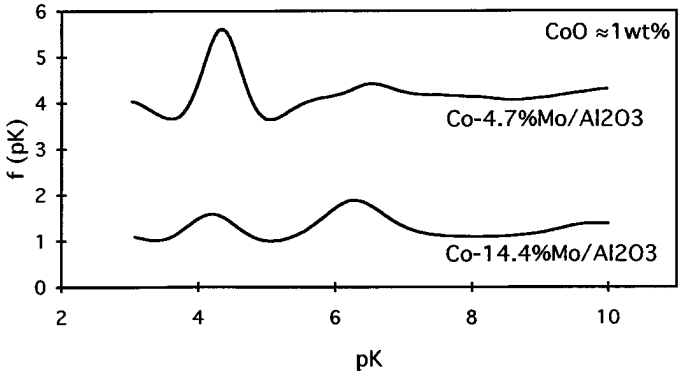

FIG. 7. Proton affinity distribution of Co-Mo/Al_2O_3 catalysts as a function of Mo content. Both samples prepared by successive impregnation of the same amount of Co on the Mo/Al_2O_3 which has different Mo content.

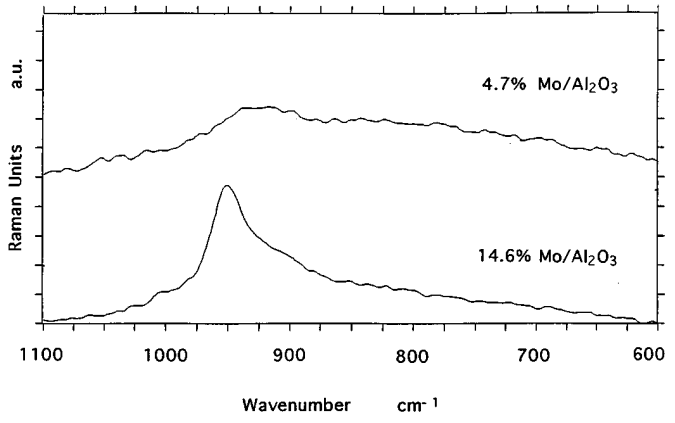

FIG. 8. Raman spectra of Co-Mo/Al_2O_3 catalysts as a function of Mo content. Both samples prepared by successive impregnation of the same amount of Co on the Mo/Al_2O_3 which has different Mo content.

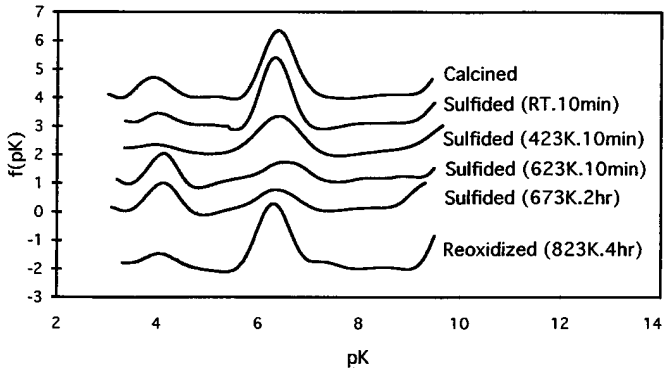

FIG. 9. Proton affinity distribution as a function of presulfiding conditions. Presulfiding was conducted in 30 ml/min flow of 10% H_2S/90% H_2 gas.

This observation suggests that the species formed during catalyst preparation and calcination can be transformed reversibly following the sulfidation/oxidation sequence.

DISCUSSION

The structure of a series of Co-Mo/Al_2O_3 catalysts in the oxide state has been studied using EXAFS (16, 32). The results indicated that octahedral molybdate was distorted and the distortion was decreased by the addition of Co to the Mo/Al_2O_3 catalyst. Taking into account these facts, we propose that Co selectively interacts with octahedral molybdate on the surface and stabilizes the surface phase. In other words, octahedral molybdate is needed to create the precursor of the HDS active site.

Collectively the results shown in Figs. 7 and 8 demonstrate that the structure and concentration of the supported Mo affects the creation of Co-Mo interaction species. Raman data suggest that the octahedral molybdate species, which is assigned to the peak around 950 cm^{-1}, are found in large amount on the ~15 wt% Mo/Al_2O_3 catalyst. PAD results suggest that creating the interaction species during impregnation of Co is more effective at higher Mo loading compared to lower loading where tetrahedral molybdate species dominate (22).

Evidence has been presented here and in our earlier work (22) that a new surface species can be identified using PADs of Co-Mo/Al_2O_3 catalytic materials. The concentration of this surface compound is controlled by several interrelated factors which we also find determine the HDS activity of the materials formed. For instance, as shown in Fig. 3 and 6, the variation of activity versus either the Co content or the pH of the Co impregnation solution follows the same trend as the number of proton binding sites with pK ~ 6 accessed from PADs. Previous researchers have also reported characterization data of HDS catalysts in the oxidic state and have proposed the existence of a Co-Mo interaction species (11, 12, 13, 15, 18, 26–28, 33–35). These earlier reports have used various spectroscopic techniques and results have prompted suggestions of the structure of the active phase(s) and precursor(s) to be proposed. Our experimental approach is based on the proton chemistry that occurs at the aqueous surface of various catalytic materials as a response to a change in the solution pH. Literature in this area supports the fact that transformation of species via Scheme **II** finds a direct analogy to homogeneous transformation of unsupported TMOs (23, 25). The factors related to this chemistry can be used to provide additional insight into the structure(s) of the supported precursor(s) which could produce the active component(s) after sulfidation.

The pH of the Co solution affects the activity and the number of proposed active site precursors, as shown in Fig. 6. It is well known that molybdate species are transformed under homogeneous conditions according to pH and concentration (25). At pH values above 7 or 8 the tetrahedral monomeric molybdate ion is present. As the pH is lowered below ~ 5.5, structures of the form $Mo_7O_{24}^{6-}$ and $Mo_8O_{26}^{4-}$ are known. At lower values of pH, heptamers with the general formula $Mo_7O_{24-z}(OH)_z^{(6-z)-}$ have been proposed based on potentiometric titration data (25). These structures are crystallographically less well-defined than that of $Mo_7O_{24}^{6-}$. At very low pH values, the structures aggregate.

Deo and Wachs reported that the structure of the supported TMO on the surface was affected by environmental conditions (23). By analogy with our WO_3/Al_2O_3 study (20), the supported molybdate can be transformed into different structures as the pH of the impregnation solution is changed (see scheme **II**) and different species could be created on the surface after drying and calcining. Figure 6 shows the maximum activity and the maximum number of the proposed active site precursors were obtained with pH ~5 during preparation. In this pH range a surface molybdate octahedral structure can be formed by hydrolysis because the impregnation solution containing Co was adjusted to that value.

The effects of Co content at a fixed Mo loading of ~15 wt% on the activity and the number of the proposed active site precursors are shown in Fig. 2. Both curves have a maximum at a Co content of 4.6 wt%. A consistency exists between the activity and the number of the sites determined from PADs. We examine the trend in the Co dispersion by XPS in a manner that parallels the above observations. Up to a certain Co loading, the dispersion increases monotonically with an increase in total Co amount and at a Co loading of 4.6 wt%, the dispersion saturates. The color of the catalyst, whose Co content is 6.7 wt%, is black, although the others are blue. This suggests the deposition of Co oxide on the surface of this catalyst. An analogy exists for Ni-Mo/Al_2O_3 catalysts. Payen *et al.* (36) reported LRS data at fixed Mo loading (14 wt% Mo) as a function of Ni content; NiO (3.6 wt%) was well dispersed but when the loading was increased to 7.2 wt% aggregated species were formed

on the surface. TPR data also support this suggestion. As the total Co content increases up to 4.6 wt%, the area under the TPR profiles increases linearly while the peak temperature decreases slightly (~40 K). Brito and Laine (37) reported a similar decrease in their study of Ni-Mo/Al_2O_3 catalysts and concluded that up to a 5 wt% loading it facilitated the reduction of Mo. In our case the profile of TPR curves changes and a new peak appears around 650 K when the Co content is 6.7 wt%. We find (Fig. 4) the position of this new peak is the same as that of a Co/Al_2O_3 catalyst. In an ESR study Gour *et al.* (38) reported that Co on alumina is easily reduced at 673 K. Chin and Hercules (39) found that Co in Co-Mo/Al_2O_3 catalysts with high weight loading of Co could be easily reduced and attributed this to the presence of Co_3O_4 on the catalyst. Arnoldy *et al.*, in a series of TPR studies relevant to this work (40, 41) reported that four different reduction regions can be present on CoO/Al_2O_3, depending on its weight loading and calcination temperature. With increasing Co content and after calcination at a temperature near the one used here, two phases of Co appear at temperatures less than 900 K. These two, which occur in the range of 650–750 K, were attributed to Co_3O_4 crystallites and Co^{3+} ions in surface positions or in a crystalline Co^{3+}-Al^{3+}-oxide of proposed stoichiometry Co_3AlO_6. Arnoldy *et al.* (42) also reported TPR results for Co-Mo/Al_2O_3 catalysts and concluded that the reducibility of Co ions is strongly influenced by the presence of Mo. Collectively these facts suggest that the catalyst containing 6.7 wt% Co has an aggregated Co oxide phase.

We propose the following line of reasoning: Co selectively interacts with a previously supported octahedral molybdate phase (Raman data for ~15 wt% Mo sample) for loadings less than ~5 wt% Co which represents a limiting capacity of the Mo/Al_2O_3 for accepting a Co ion. Above this loading of Co we assume that the "excess" Co is transformed into an aggregated Co oxide and the oxide covers the Co–Mo interaction species after calcination. The decrease in the number of the sites shown in Figs. 2 and 3 is, therefore, proposed to be the result of the blockage of the dispersed sites by the aggregated Co oxide.

The speculation that the active site precursor consists of octahedral molybdate and dispersed Co can be reexamined on the basis that the Co ion and molybdate ion can form the heteropoly ion, $[CoMo_6O_{24}]^{-10}$. A structure containing MoO_6 octahedra joined by shared edges has been proposed by Anderson for heteropolyacids whereby six MoO_6 octahedra are arranged by corner sharing with each of two neighboring octahedra such that a hexagonal $Mo_6O_{24}{}^{6-}$ annulus is built (43). The central cavity of the structure is then the same size and shape of one of the MoO_6 octahedra and can accommodate another (hetero) cation in the same sixfold coordination.

The occurrence of heteropolymolybdate species in the oxidic form of the HDS catalyst was previously proposed based on Raman spectroscopy data (44). A linear relationship between the content of the heteropolyacid impregnated on Al_2O_3 and HDS activity was also shown (33). It was reported that heteropolymolybdates are stable in the neutral pH range and they decompose in strongly acidic and moderately basic solutions (45). In the pH range used for preparation of our catalyst, the cobalt heteropolymolybdate species are stable. Our findings concerning the pH influence on the activity and PAD are therefore consistent with the possible occurrence of stable cobalt heteropolymolybdates on the catalysts.

Wivel *et al.* reported a relationship between HDS activity and absolute amount of octahedral Co in Co-Mo/Al_2O_3 catalysts in the oxide state (10). They distinguished octahedral Co in Co-Mo/Al_2O_3 from Co in Co_3O_4 and tetrahedral Co in $CoAl_2O_4$ using Mössbauer emission spectroscopy. On the basis of their data, the absolute amount of the octahedral Co reached a maximum (27 mg/g-Al_2O_3) at 0.7 of Co (total)/Mo atomic ratio and the HDS activity also had a maximum. The Co (octa)/Mo atomic ratio can be calculated by using these results and we obtain a value of 0.47. This value is consistent with a Co/Mo value of 0.5 obtained, assuming that the active phase precursor is a bidimensional layer (see below) of polycondensed units with the Anderson structure. In the isolated Anderson unit of $[CoMo_6O_{24}]^{10-}$, the Co/Mo atomic ratio is 1/6. However, when a very large number of such structures are condensed by sharing edges and corners, the resulting polymeric layer is made of [Mo-Co-Mo] units which are repeated regularly. The corresponding Co/Mo atomic ratio ($\frac{1}{2}$) becomes closer to the 0.47 value obtained from Wivel's data. This finding is consistent with our proposal that the HDS active site precursor consists of Co in the octahedral state and molybdate octahedra arranged in a two-dimensional surface structure in a manner similar to that originally proposed by Anderson for a heteropolyacid composed of Co and Mo.

To be accepted, the above proposal requires additional information related to the conformation of Mo species on the surface when its weight loading is ~15% and before Co is added. For MoO_3/Al_2O_3 catalysts in the concentration range corresponding to a Mo monolayer on alumina (approximately (40–60) $\times 10^{13}$ Mo cm^{-2}), molybdenum species are well dispersed on the surface (34). For the ~15 wt% catalyst, the calculated surface concentration of Mo is 33×10^{13} cm^{-2}. At this loading level the initial impregnation of molybdenum on alumina is expected to generate a monolayer of dispersed molybdate species which we propose generate the anchoring sites for cobalt in a subsequent impregnation. This proposal is strengthened by the observation that from the point of view of electrostatics the Co^{2+} species in the impregnating solution will have a high affinity for a counter ion with a high charge (e.g., $Mo_7O_{24}{}^{6-}$) bound to the surface. Spanos and Lycourghiotis (46) have also reported that a mutual promotion exists

in the adsorption of Mo(VI) and Co^{2+} species on alumina in the pH range 4.1–6.1 which was attributed to the strong lateral interactions exerted between the deposited Mo(VI) and Co^{2+} species. Our previous results (22) showed that the Co-Mo catalysts prepared by impregnating Mo first and Co second contain the highest amount of Co-Mo interaction species (as evidenced by PADs) and are the most active in HDS when compared with Mo-Co samples, obtained by successive impregnation in the reverse order (22). For the latter samples, impregnation of Co on bare alumina would lead to aggregated Co species which are not likely to efficiently form dispersed Co-Mo interaction species. Summarizing our reasoning to this point we have provided evidence that the preexistance of a dispersed monolayer of polycondensed molybdates during impregnation of Co is a sufficient condition for the formation of Co-Mo species, possibly with an Anderson-type structure. We have proposed that these species are responsible for the feature at pK 6 in PAD which is formed by addition of Co to Mo/Al_2O_3 catalysts.

The effect of mild sulfidation is to reduce the intensity of the peak (cf. Fig. 9) which we proposed is the result of formation of a Co-Mo-S structure whose proton chemistry is different from that of its oxidic counterpart. After more severe sulfidation the feature at pK $\sim$ 6 decreases further in intensity while an alumina feature (20–22) around pK $\sim$ 4 reappears and grows gradually. This is likely due to the cleavage of alumina-molybdate bonds and formation of a Mo sulfide phase and bare alumina sites. The effect of sulfidation could be reversed by subjecting the samples to an oxidizing atmosphere (823 K for 4 h in air). The PAD of the reoxidized catalyst is very close to that of the originally calcined one.

These results are consistent with those IR studies that showed that the OH bands due to Al_2O_3 in IR spectra were partially suppressed by impregnation of Mo (47) and were regenerated either after reduction or sulfiding MoO_3/Al_2O_3 catalysts (48).

The processes described above are reversible, in that reoxidation of presulfided catalysts reproduces PADs of fresh, calcined catalysts. Based on the argument that Co was dispersed in the fresh catalyst, we propose that the dispersed state of Co is conserved in the sulfided catalyst, too, and is recovered by reoxidation. This proposal is in agreement with other results from the literature (9).

CONCLUSIONS

The findings of this study are summarized as follows: (1) A Co-Mo interaction species can be identified in the oxide state by using PADs. (2) The amount is proportional to the thiophene hydrodesulfurization activity after sulfiding. (3) Based on the combination of Raman and XPS data, this species consists of octahedral molybdate (Raman) and dispersed Co (XPS) which, we propose, is also octahedrally coordinated. (4) Arguments have been presented based on our results and those in the literature that are consistent with the proposal that the active phase precursor in the oxide catalyst has a bidimensional monolayer structure which could be formally derived from that proposed by Anderson for cobalt heteropolymolybdate species. (5) Our proposed active phase precursor species can be transformed reversibly during the processes of sulfidation and reoxidation and this suggests that a Co-Mo interaction is still maintained in the sulfided state.

ACKNOWLEDGMENTS

We are indebted to Dr. John Baltrus of U.S. Department of Energy for measuring XPS and to Mr. Katsuyuki Sato and Mr. Kazuhiro Yagishita of Nippon Oil Company, Ltd. for measuring Raman spectroscopy. We gratefully acknowledge Dr. Karol Putyera, Dr. Jacek Jagiello, Dr. Teresa J. Bandosz, and Dr. Vlad T. Popa of Syracuse University for suggesting the problem and their assistance during the solution. Special thanks are due to Mr. Huang Chung-Chi and Ms. Sheeba Panayil of Syracuse University for their assistance with the data collection. Two of us (C.C. and J.A.S) acknowledge financial support from Division of Chemical Sciences, Office of Basic Energy Science under DOE Grant DE-FG02-92ER14268.

REFERENCES

1. Grange, P., *Catal. Rev.-Sci. Eng.* **21**, 149 (1980).
2. Knözinger, H., in *Proceedings, 9th International Cogress on Catalysis, Calgary, 1988* (M. J. Philips and M. Ternan, Eds.), Vol. 5, p. 20, Chem. Institute of Canada, 1988.
3. Prins, R., de Beer, V. H. J., and Somorjai, G. A., *Catal. Rev.-Sci. Eng.* **31**, 1 (1989).
4. Topsøe, H., Clausen, B. S., Candia, R., Wivel, C., and Mørup, S., *J. Catal.* **68**, 433 (1981).
5. Wivel, C., Candia, R., Clausen, B. S., Mørup, S., and Topsøe, H., *J. Catal.* **68**, 453 (1981).
6. Niemann, W., Calusen, B. S., and Topsøe, H., *Catal. Lett.* **9**, 355 (1990).
7. Louwers, S. P. A., and Prins, R., *J. Catal.* **133**, 94 (1992).
8. Kabe, T., Qian, W., and Ishihara, A., *J. Catal.* **149**, 171 (1994).
9. Crajé, M. W. J., de Beer, V. H. J., van Veen, J. A. R., and van der Kraan, A. M., Symposium of Advances in Hydrotreating Catalysts, ACS Meeting, Washington D.C., August 21–26, 1994.
10. Wivel, C., Clausen, B. S., Candia, R., Mørup, S., and Topsøe, H., *J. Catal.* **87**, 497 (1984).
11. Grimblot, J., and Bonnelle, J. P., *J. Electron Spectrosc. Relat. Phenom.* **9**, 449 (1976).
12. Gajardo, P., Grange, P., and Delmon, B., *J. Catal.* **63**, 201 (1980).
13. Topsøe, N., and Topsøe, H., *J. Catal.* **75**, 354 (1982).
14. Delannay, F., Haeussler, E. N., and Delmon, B., *J. Catal.* **66**, 469 (1980).
15. Kasztelan, S., Grimblot, J., and Bonnelle, J. P., *J. Phys. Chem.* **91**, 1503 (1987).
16. Clausen, B. S., Topsøe, H., Candia, R., and Villadsen, J., *J. Phys. Chem.* **85**, 3868 (1981).
17. Clausen, B. S., Lengeler, B., and Topsøe, H., *Polyhedron* **5**, 199 (1986).
18. Kasztelan, S., Payen, E., Toulhoat, H., Grimblot, J., and Bonnelle, J. P., *Polyhedron* **5**, 157 (1986).
19. Dufresne, P., Payen, E., Grimblot, J., and Bonnelle, J. P., *J. Phys. Chem.* **85**, 2344 (1981).
20. Contescu, C., Jagiello, J., and Schwarz, J. A., *J. Phys. Chem.* **97**, 10152 (1993).
21. Schwarz, J. A., Contescu, C., and Jagiello, J., *in* "Catalysis", Vol. 11, p. 127, Specialist Periodical Report, Royal Society of Chemistry, Thomas Graham House, Cambridge, 1994.

22. Adachi, M., Contescu, C., and Schwarz, J. A., *J. Catal.* **158**, 411 (1996).
23. Deo, G., and Wachs, I. E., *J. Phys. Chem.* **95**, 5889 (1991).
24. Contescu, C., Jagiello, J., and Schwarz, J. A., *Langmuir* **9**, 1754 (1993).
25. Baes, C. F., and Mesmer, R. E., "The Hydrolysis of Cations," p. 237, Wiley & Sons, New York, 1976.
26. Okamoto, Y., Imanaka, T., and Teranishi, S., *J. Catal.* **65**, 448 (1980).
27. Medema, J., van Stam, C., de Beer, V. H. J., Konings, A. J. A., and Koningsberger, D. C., *J. Catal.* **53**, 386 (1978).
28. Cheng, C. P., and Schrader, G. L., *J. Catal.* **60**, 276 (1979).
29. Hu, H., Wachs, I. E., and Bare, S. R., *J. Phys. Chem.* **99**, 10897 (1995).
30. Rönngen, L., Sjöberg, S., Sun, Z.-X., Forsling, W., and Schindler, P. W., *J. Colloid Interface Sci.* **145**, 396 (1991).
31. Sun, Z.-X., Forsling, W., Rönngen, L., Sjöberg, S., and Schindler, P. W., *Colloid Surf.* **59**, 243 (1991).
32. Chiu, N.-S., Bauer, S. H., and Johnson, M. F. L., *J. Catal.* **89**, 226 (1984).
33. Spojakina, A., Kardjieva, R., Damyanova, S., and Shopov, D., *in* "Proceedings, 5th Int. Symp. Heterogeneous Catalysis, Varna, 1983," p. 353.
34. Richardson, J. T., *I.E.C. Fundamentals* **3**, 155 (1964).
35. Ratnasamy, P., and Knözinger, H., *J. Catal.* **54**, 155 (1978).
36. Payen, E., Grimblot, J., and Kasztelan, S., *J. Phys. Chem.* **85**, 2344 (1981).
37. Brito, J. L., and Laine, J., *J. Catal.* **139**, 540 (1993).
38. Gour, P. K., and Tiwari, J. S., Upadhyay, S. N. U., Pande, S., Ghosh, O. K., Bhattacharyya, N. B., and Sen, S. P., *in* "Procedings, 4th Climax International Conference on the Chemistry and Uses of Molybdenum (H. F. Barry and P. C. H. Mitchell, Eds.), p. 367, Climax Molybdenum Golden Co.," 1982.
39. Chin, R. L., and Hercules, M., *J. Phys. Chem.* **86**, 3097 (1982).
40. Arnoldy, P., and Moulijn, J. A., *J. Catal.* **93**, 38 (1985).
41. Arnoldy, P., de Booys, J. L., Scheffer, B., and Moulijn, J. A., *J. Catal.* **96**, 122 (1985).
42. Arnoldy, P., Franken, M. C., Scheffer, B., and Moulijn, J. A., *J. Catal.* **96**, 381 (1985).
43. Anderson, J. S., *Nature (London)* **140**, 850 (1937).
44. Jeziorowski, H., and Knözinger, H., *Appl. Surf. Sci.* **5**, 335 (1980).
45. Matijevic, E., and Kerker, M., *Inorg. Chem.* **2**, 581 (1963).
46. Spanos, N., and Lycourghiotis, A., *Langmuir* **10**, 2351 (1994).
47. Okamoto, Y., and Imanaka, T., *J. Phys. Chem.* **92**, 7102 (1988).
48. Millman, W. S., Segawa, K., Smrz, D., and Hall, W. K., *Polyhedron* **5**, 169 (1986).